MEMS Pressure Sensor Array for Aeroacoustic Analysis of the Turbulent Boundary Layer

Joshua S. Krause* and Robert D. White†
Tufts University, Medford, MA, USA

Mark J. Moeller, ‡
Judith M. Gallman,§ and Gerard Holup¶
Spirit AeroSystems Inc., Wichita, KS, USA

Richard De Jong‖
Calvin College, Grand Rapids, MI, USA

The second stage of the design, fabrication, and characterization of a surface micromachined, front-vented, 64 channel (8×8), capacitively sensed pressure sensor array is described. The array was fabricated using the MEMSCAP PolyMUMPs® process, a three layer polysilicon surface micromachining process with an additional fabrication step using Parylene-C. An acoustic lumped element model was used to model an individual microphone and then applied to the array as a whole. The computational results for the design, including mechanical components, environmental loading, fluid damping, and other acoustic elements are detailed. Theory predicts single element sensitivity of 0.65 mV/Pa at the gain stage output in the 100-40,000 Hz band. A laser Doppler velocimetry (LDV) system has been used to map the spatial motion of the elements in response to electrostatic excitation. A strong resonance appears at 410 kHz for electrostatic excitation, in agreement with mathematical models. Static stiffness measured electrostatically using an interferometer is 0.1 nm/V^2, similar to the expected stiffness. Preliminary acoustic sensitivity studies show average single element acoustic sensitivity of 0.6 mV/Pa from 200 to 20 kHz. A more in depth analysis of acoustic sensitivity is ongoing as well as element-to-element variability.

Nomenclature

a	Radius of diaphragm
a_{eff}	Effective radius of diaphragm
t_{dia}	Thickness of diaphragm
a_{gap}	Radius of the gap cavity
t_{gap}	Thickness of air gap
V_{gap}	Volume of air gap
n	Number of holes in the diaphragm
a_{hole}	Radius of diaphragm vent holes
C_c	Center–to–center spacing of vent holes
ρ	Density of air
c	Speed of sound
μ	Viscosity of air
ρ_1	Density of diaphragm (Polysilicon)
E_1	Modulus of elasticity of diaphragm
ν_1	Poisson's ratio of diaphragm

*Research Assistant, Department of Mechanical Engineering; Joshua.Krause@tufts.edu
†Assistant Professor, Department of Mechanical Engineering, AIAA Member
‡Acoustic Analyst, AIAA Member
§Associate Technical Fellow, AIAA Member
¶Acoustic Laboratory Technician
‖Professor, Department of Mechanical Engineering

t_2 Thickness of Parylene-C layer
ρ_2 Density of Parylene-C layer
E_2 Modulus of elasticity of Parylene-C layer
ν_2 Poisson's ratio of Parylene-C layer
D_{eff} Effective stiffness of thin bending plate
V_{bias} Bias voltage applied
ϵ_0 Permittivity of free space
C_fb Feedback capacitor in charge amplifier
R_fb Feedback resistor in charge amplifier
R_{stray} Stray resistance between diaphragm and metal trace
C_{block} DC blocking capacitor
R_{block} Resistor to ground after DC blocking capacitor
f_b Break frequency for AD621
R_{A1} Lumped element resistance 1 due to air
R_{A2} Lumped element resistance 2 due to air
M_{A1} Lumped element mass loading due to air
C_{A1} Lumped element compliance due to air
C_{cav} Lumped element compliance of the cavity
C_{dia} Lumped element compliance of the diaphragm
M_{dia} Lumped element mass of diaphragm
R_{th} Lumped element resistance through holes in the diaphragm
S Škvor's formula
C_f Correction factor to Škvor's formula
R_{sq} Lumped Element resistance due to squeeze film damping
R_{hole} Lumped Element resistance of the holes in the diaphragm
N Transducer coupling parameter
U_{dia} Volume velocity of diaphragm
I Current
V_{ac} AC voltage
P Electrostatic pressure

I. Introduction

Turbulence has been plaguing transport aircraft designers for over fifty years. Tennekes and Lumley pose seven qualities that characterize turbulence. They present turbulence as being irregular, diffuse, and often associated with large Reynolds numbers. It is a three-dimensional vortical fluctuation following a continuum model and dissipates over time.[1] Several models have been analytically and experimentally obtained to understand the complex nature of turbulence, but as a result of the stochastic nature, a theoretical model is more difficult to obtain. Therefore, using hot wire anemometry, shear stress sensors, and pressure sensors at the microscopic level will help to obtain empirical results describing the phenomena associated with turbulence and more specifically the turbulent boundary layer (TBL).

The sources of structural excitation and radiative noise in passenger aircrafts are noise due to the interior environment, the engine, and the fluctuations in wall pressure beneath the TBL. The noise generated by the TBL is considered the most dominant noise source on transport aircrafts.[2] In order to model the structural response of an aircraft, spectral levels at both low and high wavenumbers are needed.[3] The low wavenumber assessment is vital due to the fact that structural resonances take place at low wavenumbers and acoustic noise is generally emitted at low wavenumbers compared to convective turbulent energy.[4] Although low wavenumbers are important for the analysis of acoustic noise generation and structural vibrations, the high convective wavenumbers are where the greatest energy levels are present in the turbulent field, and hence need to be understood. A lack of empirical knowledge as a result of the limits due to conventional instrumentation is one reason for our poor understanding of turbulence.[5] MEMS pressure sensors may alleviate this issue due to their small size and the ability to fabricate multiple microphones in a fine pitch array. The challenge in MEMS arrays is achieving good matching between elements in the array and across arrays. In addition, due to their small size, the microphones necessarily have low sensitivity.

MEMS pressure sensors have been explored by many researchers over the past 25 years and many review articles can be found on them.[6–8] Most pressure sensors are developed for auditory applications, biomedical ultrasound arrays, and underwater applications.[7] Few microphones have been developed for aeroacoustic applications, possibly due to the difficulty of surviving the harsh environment. The Interdisciplinary Microsystems Group at the University of Florida Gainesville has done a great deal of work in this area and Martin *et al.* demonstrate a good summary of the previous microphones for aeroacoustic measurement.[9]

II. Fabrication and Design

The fabrication process of the 64 channel capacitively sensing microphone array utilizes the MEMSCAP PolyMUMPs® process along with facilities at Tufts University in the Tuft Micro and Nano Fabrication Facility (TMNF). The PolyMUMPs process is a foundry process that fabricates polysilicon structures via surface and bulk micromachining with a minimum feature size of 2 μm. The process consists of seven physical layers, including 3 structural, 2 sacrificial and one metal layer. A photograph of a completed microphone sensor array is shown in *Figure* 3.

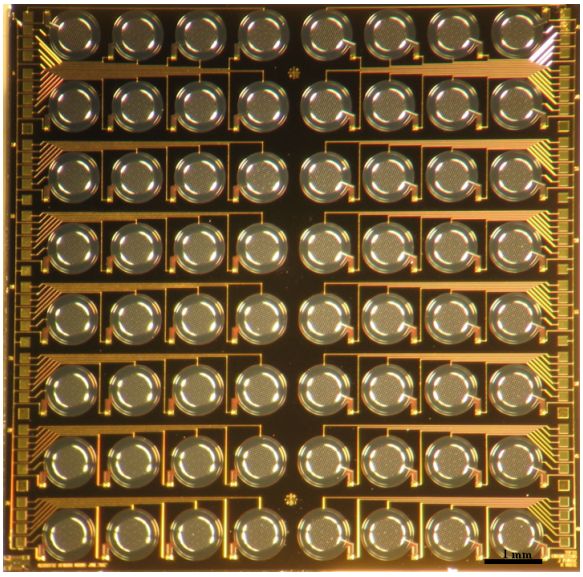

Figure 1. Photograph of the 64 microphones arrayed in an 8 × 8 pattern. Chip is 1 cm on a side. Individual elements are 0.6 mm in diameter.

The fabrication process for a single element in the array is described. The process starts with a heavily phosphorus doped 150 mm n–type silicon wafer with a <100> crystalline structure and resistivity of 1–2 ohm–cm. The process then uses low pressure chemical vapor deposition (LPCVD) to deposit a 600 nm layer of silicon nitride to isolate the electrical properties of the bulk silicon from the MEMS device. After the silicon is electrically isolated, the building of the structures is started by using the Poly 0 layer. The Poly 0 layer is a 500 nm layer of polysilicon that is also deposited by LPCVD, then patterned by photolithography to get the desired structure. After the first structural layer is deposited, a 2 μm sacrificial layer is deposited by LPCVD and annealed for 1 hour at 1050° C. This structure is removed once the entire MUMPs process has been completed. However, before the release of the structure, several layers are patterned.

After the initial deposition of the PSG (1^{st} Oxide) layer, a dimples mask is patterned by photolithography and etched out of the oxide using reactive ion etching (RIE). The depth of this etch is 750 nm. Next, the Anchor 1 mask will be patterned allowing the diaphragm to anchor to the nitride layer. The second structural (Poly 1) layer is then deposited to a thickness of 2 μm. A 200 nm PSG layer is then deposited for 1 hour at 1050° C to dope the polysilicon with phosphorus while also reducing the stress in the deposition. The Poly 1 layer is then patterned with a hard mask which allows for a higher yield when the pattern is transferred to the polysilicon.

After the Poly 1 layer, a second sacrificial (2^{nd} Oxide) layer is deposited and annealed at a thickness of 750

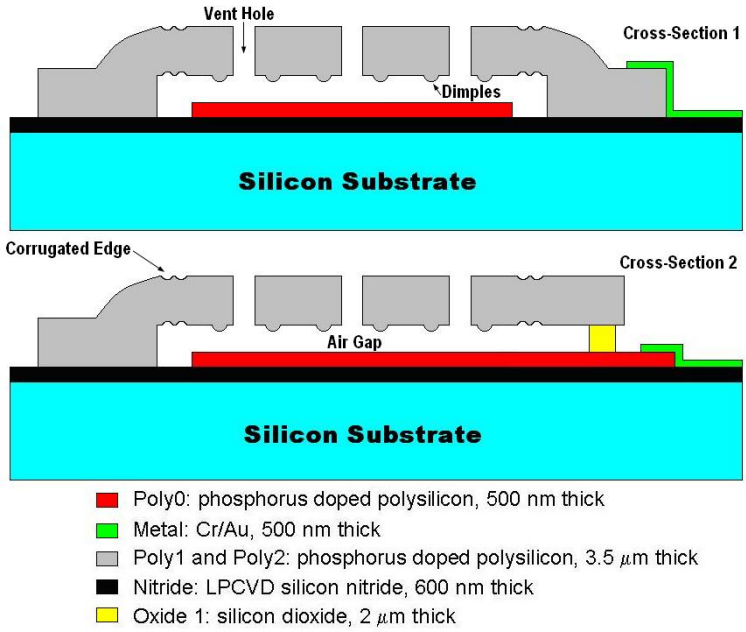

Figure 2. Schematic of one element in the microphone array showing two cross-sectional view before parylene coating. Cross-section 2 is through a region where the poly0 layer "tunnels" below the diaphragm to allow electrical connection to the bottom electrode. Cross-section 1 is through a more common region where there is no tunnel.

nm. This layer is patterned with a Poly1_Poly2_Via mask as well as an Anchor 2 mask. The Poly1_Poly2_Via layer provides etch holes to be patterned through the second oxide and the Anchor 2 mask is used to etch both the first and second oxides in one step. Following this, the final structural layer of polysilicon (Poly 2) is deposited to a 1.5 μm thickness and then patterned. The same PSG process is applied to the Poly 2 layer to dope the layer in phosphorus. The final deposition layer is the metal layer. The metal layer is a 0.5 μm layer of gold that provides an electrical connection for wiring and bonding.

Applying this process to the microphone array utilizes all layers in the process. The design for each sensor consisted of the base silicon wafer, followed by the nitride layer. The first structural layer to compose the actual sensor element is the Poly 0 layer. The Poly 0 layer is a circle with a radius of 290 μm which acts as the bottom electrode for the microphone. Poly 0 is also used to "tunnel" under the diaphragm supports (using an oxide as insulation) to create the electrical connection between the bottom electrode and the wire which leads to the common biasing pads.

After the 1^{st} Oxide layer is placed over Poly 0 layer, the Dimple layer is used to etch part of the way through the oxide 1 layer. This is used to put in place "dimples" on the bottom of the Poly 1 layer which will minimize the adhesion problems associated with stiction during the release of the structure at the end of the fabrication process. Through the use of the peel number and assuming our structure acts like a doubly supported beam, we determined the dimples associated with reducing stiction will be spaced 30 μm apart for a total of 201 dimples over the Poly 1 region.[10] Besides preventing adhesion, the dimple mask is used to create a corrugation of two concentric five micron wide circles. This corrugation allows for the partial relaxation of any residual stresses produced in the diaphragm during the fabrication process or during operation. This allows for an increase in sensitivity due to the reduction of the stress.[11] *Figure* 4 shows a scanning electron microscope image of an individual microphone in the array illustrating these design features.

The first sacrificial layer (1^{st} Oxide, 2 μm thick) is then patterned using the Anchor 1 mask. This is drawn 20 microns around the Poly 0 layer in a torus shape. The Anchor 1 layer defines the inner dimension of the diaphragm, giving the mechanical diaphragm an inner radius of 300 μm. Anchor 1 is also used to anchor the polysilicon/metal signal wires, guard bands, pads, and ground connections. Following the Anchor 1 layer, the Poly 1 layer is patterned. The Poly 1 layer is used both as the first part (2 μm of the total 3.5 μm) of the mechanical diaphragm and as part of the poly/metal wires. The Poly 1 portion of the diaphragm

has a radius of 455 μm, extending well into the Anchor region.

The next layer fabricated in the process is the Poly1_Poly2_Via layer which opens holes from the Poly1 to Poly2 layers. Due to the constraints of the bulk processing in the MUMPS process, we needed to combine the two layers (Poly1 and Poly2) to create a structure with a 3.5 μm thickness. The Poly1_Poly2_Via layer is used for this purpose; it removes the interlayer dielectric (oxide 2) so that Poly 1 and Poly 2 are directly in contact, effectively forming a single 3.5 μm thick polysilicon structural layer. The Anchor 2 layer opens holes for poly 2 directly to the Nitride or Poly0 layer. In this application the Anchor 2 is solely used to ground the elements to the substrate.

Holes are etched through both the Poly 1 and Poly 2 layers using the "hole 1" and "hole 2" layers. The hole through Poly 1 is 6 μm in diameter; the hole through Poly 2 is 4 μm in diameter. The holes have two purposes: (1) they will be used to introduce HF etchant during release to etch out the oxide 1 sacrificial layer (2) they act as frontside "vents" during operation, equalizing ambient pressure with gap pressure and providing damping.

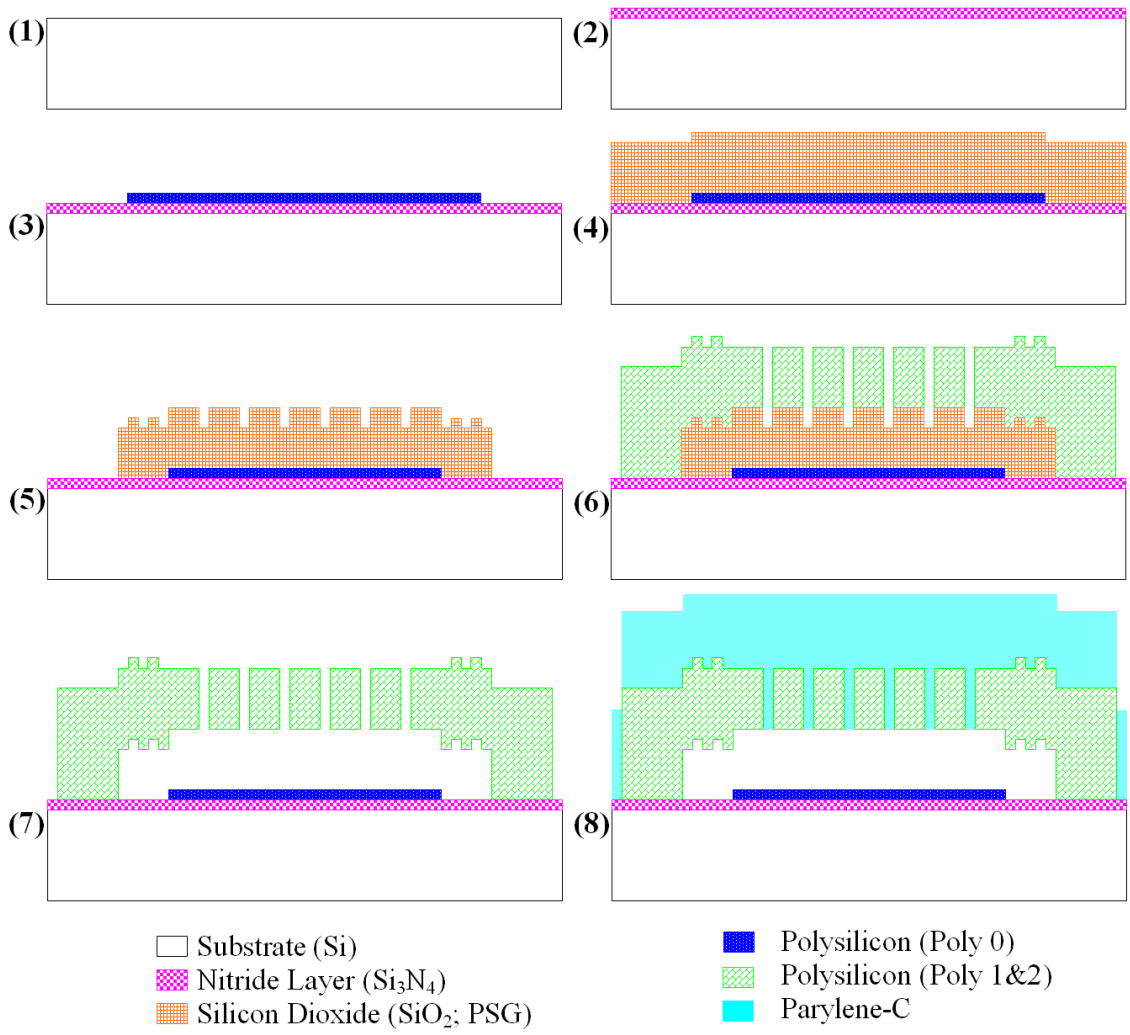

Figure 3. Schematic illustrating the fabrication process using the MEMSCAP PolyMUMPS ® process. (1) Bare silicon substrate. (2) Silicon Nitride layer is deposited as electrical isolation layer. (3) Bottom electrode is applied through Poly 0 layer. (4) Sacrificial oxide layer is deposited to create the cavity. (5) Dimples are patterned into 1^{st} Oxide layer. (6) Poly 1 and Poly 2 layers are deposited as diaphragm. (7) Oxide is removed through HF release. (8) Parylene-C is deposited and sensor fabrication is complete.

Finally the Metal layer is used as a routing layer and as electrical pads around the outside of the device. All the wires and pads are combinations of polysilicon and metal, anchored directly to the nitride layer or to the bulk silicon, as appropriate. The final design implemented guard bands to ensure electrical connections, alignment markers and extra ground connections were applied to ensure a safe dissipation of static discharges, EMI and RFI signals. A uniform process was applied to the wiring of each element with guard bands located in between each wire (where each guard band connects to a common ground).

The elements are arrayed on a 1.01 cm × 1.01 cm chip in an 8×8 pattern. There are 76 bond pads along two edges of the chip for electrical connection. The direction of flow is bottom to top so the flow does not pass across the bond pads. The element center-to-center pitch in the direction of flow is 1.2625 mm (which allows for multiple 8×8 array to be placed end-to-end to determine low wavenumber information through the larger spatial scale), while the pitch across the flow is 1.1125 mm. Packaging uses a ceramic pin grid array (CPGA) package to which the MEMS array is wirebonded. Laser cut spacers allow for the MEMS chip to be mounted flush with the package surface. Off chip electronics amplify the signal to a data acquisition enabled computer.

Post processing after MEMSCAP fabrication includes one additional polymer layer to reduce the size of the etch holes. This reduction in hole size greatly improves on our low frequency response as will be shown in the next section. However, after the PolyMUMPs® process has been completed, and before the polymer layer is deposited, the release of the sacrificial oxide is preformed. This consists of a 30 minute hydrofluoric acid (HF) etch, followed by two separate five minute deionized water rinses. After the water rinses, the arrays were place in a bath of isopropanol (IPA) for five minutes and methanol for 15 minutes to reduce the amount of surface tension when drying. When the arrays are removed from the methanol bath, they are stored in a desiccator under vacuum to dry.

The final step in the microphone array fabrication is the application of a 2 μm layer of Parylene (Poly-para-xylylene) type C which is deposited through chemical vapor deposition at the TMNF. In addition to reducing the hole size on the membrane, the Parylene-C acts as an electrical isolation for the wirebonds, connection terminals on the CPGA, as well as the on MEMS device. After the deposition, the microphone arrays are more robust and can withstand greater environmental effects, most notably resistance to moisture and temperature stability. In initial testing, the deposition of the Parylene-C layer does not come without yield issues. If the amount of Parylene-C being deposited is too large, in certain cases the vent holes and the air gap become filled with the Parylene-C which can cause stiction of the devices, greatly reducing the sensitivity. However, examples of devices where this does not occur show promising results as described in this paper.

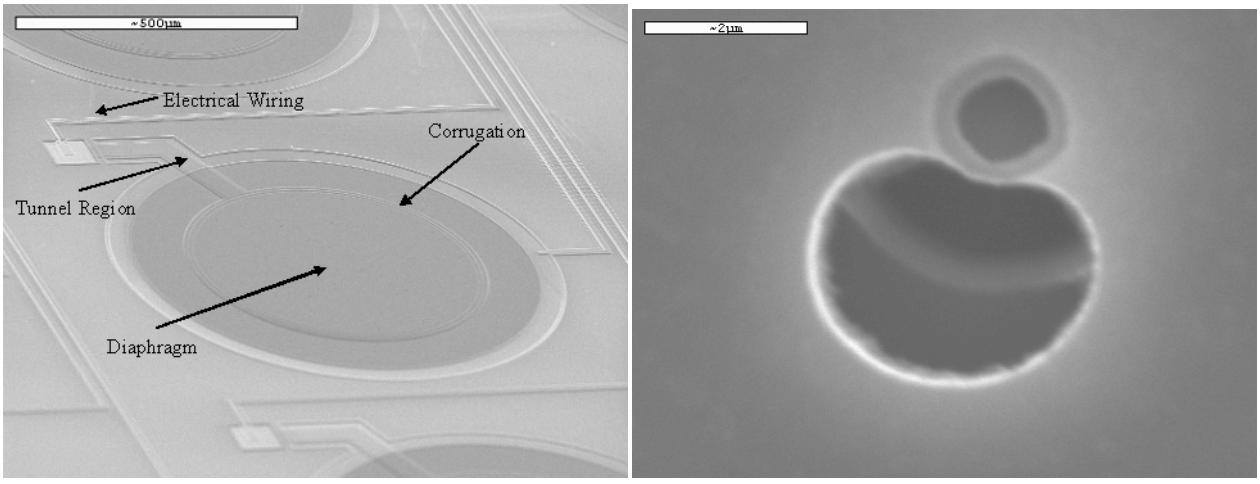

(a) (b)

Figure 4. (a) SEM image tilted at a sixty degree angle of an element illustrating the diaphragm, corrugation around diaphragm, wire scheme, and tunnel concept for electrical connection to bottom electrode. Diaphragm is 600 μm. (b) SEM image of vent hole for static equilibrium of pressure. This image was taken before Parylene coating. Parylene coating partially seals the vent hole.

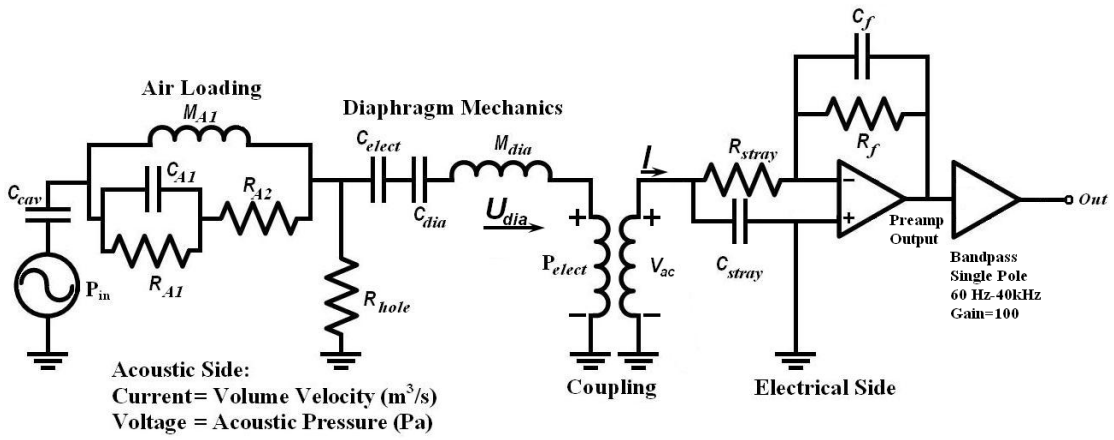

Figure 5. Coupled mechanical-electrical lumped element model.

III. Model

A model for one individual microphone in the array is described. For each element in our design, a MATLAB® script was compiled to examine the microphone's response electrostatically as well as to a unit pressure. The parameters of the script were computed using lumped elements in an acoustic analog as shown in the circuit diagram in *Figure* 5. The compliance, resistance and mass of the microphone were accounted for in the circuit diagram and then implemented into the MATLAB® script. The compliances, resistances and mass loading of the microphones were computed using parameters from.[9,12,13] Using Beranek's solutions for the environmental loading of a rigid piston in an infinite baffle, we compute:

$$R_{A1} = \frac{0.1404\rho c}{a_{eff}^2} \quad (1)$$

$$R_{A2} = \frac{\rho c}{\pi a_{eff}^2} \quad (2)$$

$$M_{A1} = \frac{8\rho}{3\pi^2 a_{eff}} \quad (3)$$

$$C_{A1} = \frac{5.94 a_{eff}^3}{\rho c^2} \quad (4)$$

$$C_{cav} = \frac{V_{gap}}{\rho c^2} \quad (5)$$

where ρ is the density of air, c is the speed of sound, a is the effective radius of the diaphragm (equal to 80% of the actual radius for a circular bending plate), and V_{gap} is the volume of the gap between the diaphragm and bottom electrode. From Martin *et al.* we compute resistance due to the holes in the diaphragm, the compliance of the diaphragm (for a two layer thin laminate clamped circular bending plate), and the effective mass of the diaphragm (for the first mode of the same two layer thin laminate clamped circular bending plate):[9]

$$R_{through} = \frac{72\mu t_1}{n\pi a_{hole}^4} \quad (6)$$

$$C_{dia} = \frac{\pi a^6}{16 * 12} * \frac{1}{D_{eff}} \quad (7)$$

$$M_{dia} = \frac{9(\rho_1 t_1 + \rho_2 t_2)}{5\pi a^2} \quad (8)$$

where μ is the viscosity of air, t_1 is the thickness of the diaphragm, t_2 is the thickness of Parylene-C, ρ_1 is the density of polysilicon, ρ_2 is the density of Parylene-C, n is the number of holes in the diaphragm, a_{hole} is the radius of the holes in the diaphragm, a is the radius of the diaphragm, and D_{eff} is the effective bending

stiffness of the Parylene-C and the polysilicon diaphragm.

$$D_{eff} = \sum_{i=1}^{I} \frac{E_i}{1-\nu_i^2}\left(\frac{t_i^3}{12} + t_i y_i^2\right) \tag{9}$$

$$y_c = \frac{\sum_{i=1}^{I} z_i\left(\frac{E_i}{1-\nu_i^2}\right)}{\sum_{i=1}^{I} \frac{E_i}{1-\nu_i^2}} \tag{10}$$

$$y_i = z_n - y_c \tag{11}$$

where i is the layer type (polysilicon or Parylene-C), ν_i is Poisson's ratio for each layer, E_i is the elastic modulus of each layer, y_c is the position of the neutral axis, y_i is the distance from the center the layer to the neutral axis, and z_i is the position of the center of the i^{th} layer with respect to the reference height. Next we can use Škvor's formula, (S), and calculating a correction factor, (C_f) we can determine the resistance due to the squeeze film damping (R_{sq}).[9,14]

$$S = \frac{\pi a_{hole}^2}{C_c^2} \tag{12}$$

$$C_f = \frac{S}{2} - \frac{S^2}{8 - \frac{1}{4}ln(S) - \frac{3}{8}} \tag{13}$$

$$R_{sq} = \frac{12\mu C_f}{n\pi t_{gap}^3} \tag{14}$$

The hole resistance in the circuit model is the series combination of the squeeze film damping, R_{sq} and the through-hole damping, R_{th},

$$R_{hole} = R_{sq} + R_{th} \tag{15}$$

where C_c is the center-to-center spacing of holes in the diaphragm. Using the above model for the microphone and using a coupling parameter, N, to relate the pressure to a voltage:

$$N = \frac{V_{bias}\epsilon}{t_{gap}^2} \tag{16}$$

where V_{bias} is the bias voltage applied to the bottom electrode, ϵ is the permittivity of free space, and t_{gap} is the height of the air gap. This coupling parameter gives the acoustic pressure applied to the diaphragm for a given AC voltage on the electrical side, and, equivalently, the current into the electrical side in response to a given volume velocity of the diaphragm.

$$P = N \cdot V_{ac} \tag{17}$$

$$I = N \cdot U_{dia} \tag{18}$$

The sensitivity (voltage out per Pascal) can be computed as a function of frequency by incorporating the electronics which give the response curve its shape. The model for the receive electronics is a series combination of two single pole passive high pass filters with break frequencies of 60 Hz and 80 Hz, a charge amplifier with a gain of 100 mV/pC, and a voltage gain stage of 100 with a single pole low pass filter at 40 kHz. The final predicted pressure sensitivity results are shown in *Figure* 6. This is sensitivity at the bandpass output (40 dB above the preamp output in the passband). As shown in *Figure* 6, varying the size of the vent holes has a major impact on the low frequency response. As designed, with 1 μm radii vent holes, the sensitivity has a flat frequency response over the human frequency range for which the microphone was designed for. The additional models for 0, 2 and 3 μm vent hole sizes are shown due to the irregular sizes shown in 4. The predicted response with the misaligned vent holes (thus increasing the size of the vent holes to 2 or 3 μm), decrease the low frequency response, whereas completely covering the holes (0 μm vent holes) by including the Parylene coating slightly increases the low frequency response. The sole concern with covering the vent holes completely is the effect that if the static pressure changes, the microphone would burst.

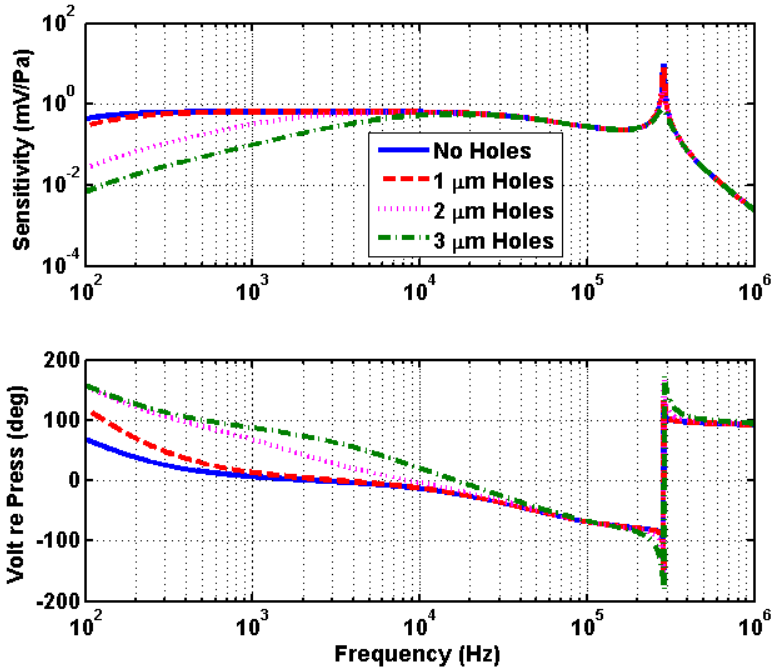

Figure 6. Predicted acoustic sensitivity for a single element with 9 V_{bias}, showing the importance of the vent hole size. Hole sizes are shown with radii of 0, 1, 2 and 3 μm.

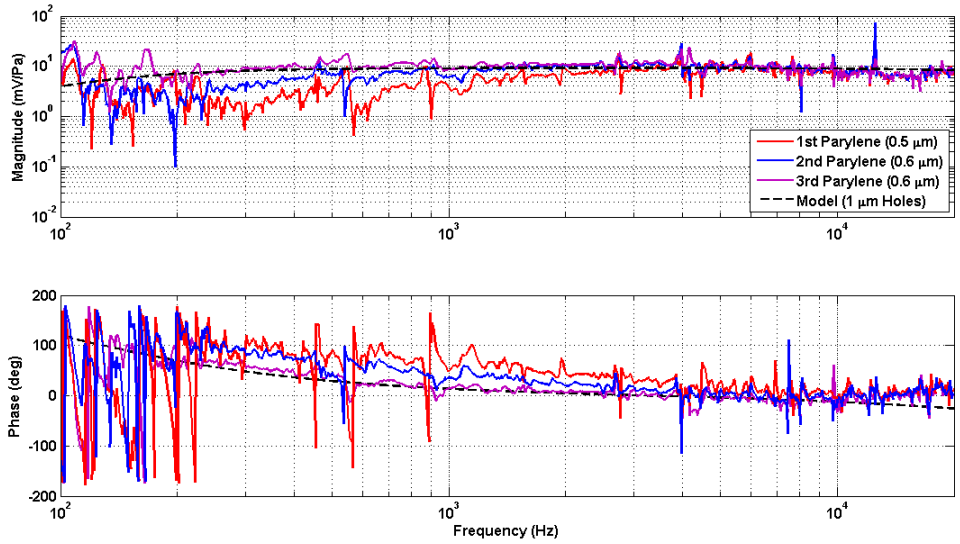

Figure 7. Sensitivity results after the Parylene-C layer is deposited onto the microphone array.

IV. Results

Although the above computational models include variations for unexpected results from the fabrication process, the fabrication process is considered a success due to the fact that there was no stiction of the membrane in normal release circumstances, no buckling of the membrane, static stiffness measurements due to membrane displacement corresponded close to theoretical predictions, and sensitivity to sound could be measured. That being stated, examples of design constraints that were not met are the minimum feature

size of 2 μm, alignment of mask layers, a thinning of the silicon nitride layer, and etch times for releasing the oxide layer. *Figure* 4 demonstrates some of the features of the microphone array after fabrication. As seen in *Figure* 4b, the largest problem to which has vast implications in the dynamics of the model is the alignment and increase in size of the vent holes in the diaphragm. The alignment issue was first a concern to whether the sacrificial oxide layer could be removed to release the membrane.

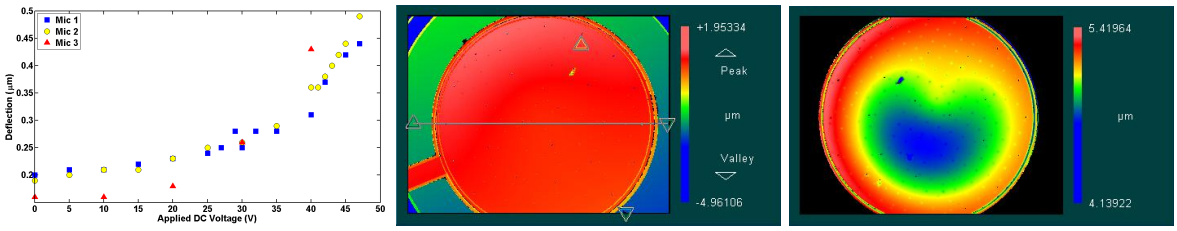

(a) (b) (c)

Figure 8. (a) Plot of center point displacement as a function of voltage right before snapdown, (b) White light interferometer screenshot showing membrane with 0 volts applied, and (c) White light interferometer screenshot showing membrane with 47 volts applied causing snapdown

Several tests have been performed to validate that this is not the case. Capacitance tests before and after release indicate a reduction in capacitance which confirms the silicon dioxide has been removed and the membrane has been released. A non-contact white light interferometer measured the surface topology as a DC voltage was applied to the membrane to determine when snapdown would occur. The empirical results from this measurement followed closely to the theoretical results and is shown in *Figure 8a*. *Figure 8a* shows three different elements all showing a snapdown voltage close to 47V, precisely the voltage at which the membrane theoretically snaps down. These tests confirm that the membrane has been released.

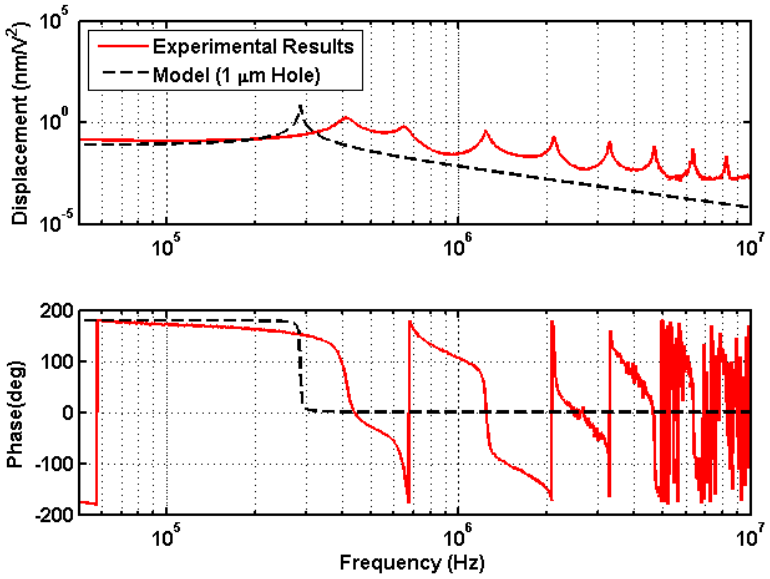

Figure 9. Laser Doppler velocimetry (LDV) measurements as a result of an electrostatic excitation to the microphone.

Laser Doppler velocimetry (LDV) is used to measure the centerpoint vibration of the diaphragm in response to an applied AC voltage plus DC bias. The results of the measurement show a strong, high Q resonance at 410 kHz (theory predicts a resonance at 285 kHz). The frequency of the resonance is strongly influenced not only by the bending stiffness of the diaphragm, but also by the acoustic stiffness coming from the backing cavity and the environmental acoustic impedance. *Figure* 9 shows a comparison between the measured electrostatic frequency response and the model predictions. The model does a good job of predicting the primary resonance frequency and the shape of the low frequency magnitude curve. At high frequencies, the LDV measurement shows many higher order modes of vibration of the membrane. It should

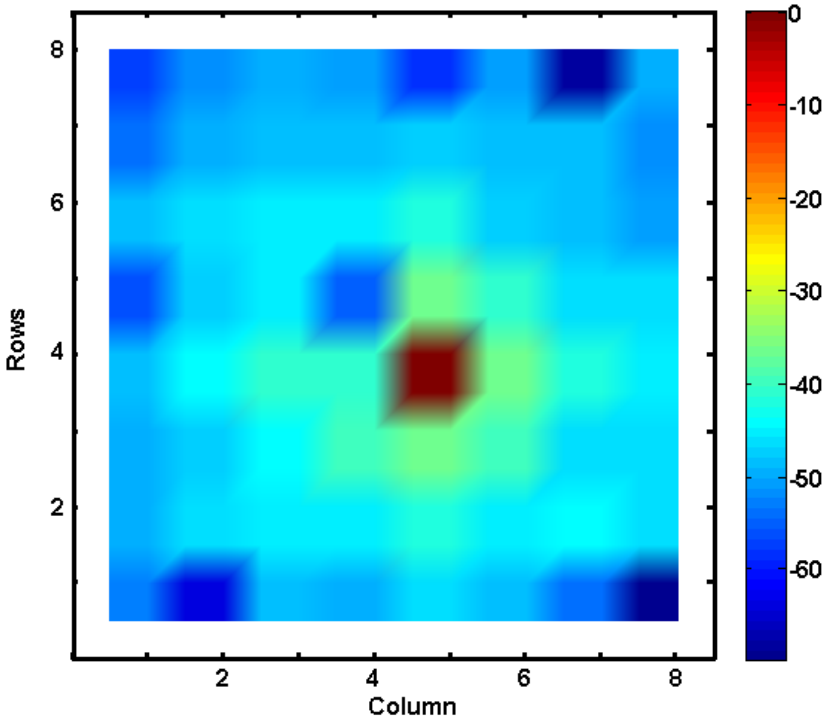

Figure 10. Laser Doppler velocimetry (LDV) measurements for the entire array when a single microphone in the middle of the array is excited. A $5V_{AC} + 5V_{DC}$ was applied to the microphone and the isolation between the microphones in the array was recorded. The colormap shows the rejection (in dB) between microphone channels.

be noted that the mathematical model only includes the first mode of membrane vibration. Another aspect for which LDV can be used is to measure the cross channel static isolation from microphone to microphone. *Figure* 10 shows the response of the entire array as a single microphone is excited electrostatically. The colormap shows at least a 30 dB rejection from the excited element for adjacent microphones to a 70 dB rejection from microphones at the edges of the array. From this test alone it is not possible to determine whether the 30 dB cross-talk between adjacent elements is from electrical cross-talk between channels, or acoustic cross-talk through either the substrate or the air.

Two methods of acoustic calibration were used. First, a free field calibration was used, followed by a plane wave tube calibration. The free field calibration limits the sound pressure level during the experiments but allows testing to high frequencies. The plane wave tube limits the measureable frequency due to cross modes at the cutoff frequency (determined by the cross section of the tube), but allows testing of larger sound pressure levels. In the free field setup, *Figure* 11a shows the response is linear as the bias voltage is increased. These tests are done inside a Faraday cage to reduce electromagnetic interference (EMI) from the speaker drive. The linear increase of sensitivity with bias is a strong indication that the microphone array is, indeed, sensing sound, and not just picking up EMI. The sensitivity at the bandpass output with 9 V_{bias} is on the order of 10 mV/Pa at 1 kHz for 14 elements in parallel (0.7 mV/Pa for a single element), similar to model predictions. The sensitivity measurements for 14 elements in the array are shown in *Figure* 11b and are tested in a Faraday cage with the MEMS microphone array placed face-to-face against a Brüel & Kjær Type 4939 1/4-inch free-field microphone. The acoustic response is very similar to model predictions across the band, and demonstrates that the array is sensitive out to at least 20 kHz. *Figure* 7 shows sensitivity results as the Parylene-C layer increases in thickness to an ideal case of about 2 μm, illustrating the importance of the smaller vent holes to regain the low frequency response.

Plane wave tube testing was conducted to reach high enough sound pressure levels to test individual microphone sensitivity. In this test, the microphone array is mounted flush with the sidewall of the square

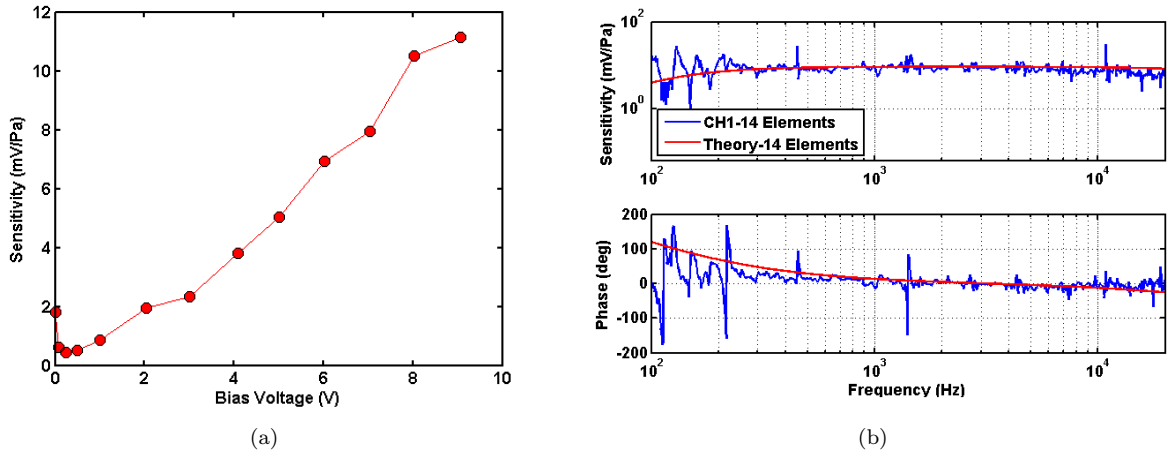

(a) (b)

Figure 11. Plots of 14 elements (in parallel) of MEMS device versus a type 4939 B&K microphone tested in a Faraday cage using face-to-face setup. (a) Plot shows that sensitivity increases as bias voltage increases, thus indicating measuring actual response rather than electrostatic interference. (b) Plot shows values in close accordance with theoretical values.

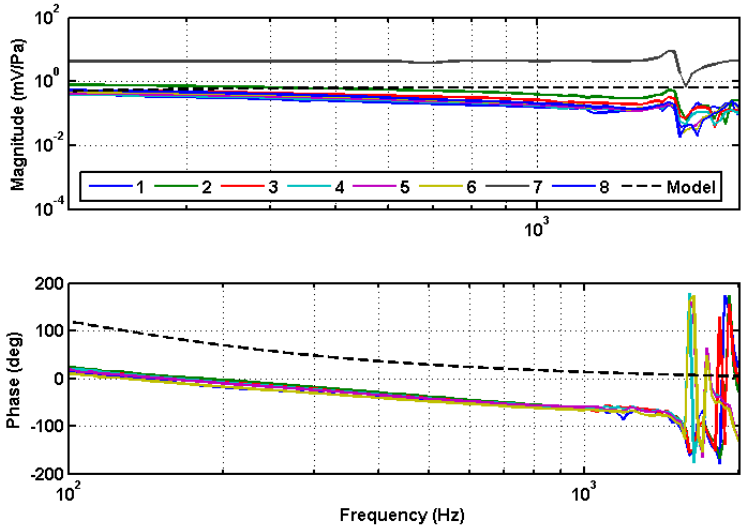

Figure 12. Sensitivity results for eight individual elements in a plane wave tube.

plane wave tube. A Brüel & Kjær 1/4-inch microphone is mounted immediately opposite the center of the array, with the microphone diaphragm flush with the inside sidewall. In individual microphone testing we see similar features to the free field results (increase in sensitivity with bias and similar magnitudes when extrapolating individual microphone performance). This can be seen in *Figure* 12, where eight individual microphones are measured in one column (parallel to the impinging acoustic wave) on the array. The microphone response is flat at low frequencies until it reaches 2 kHz, where higher cross-modes or other acoustic effects begin to appear in the calibration curve. Microphone #7 shows a much higher sensitivity than the other 7 microphones in this column. The cause of this is not known. The other 7 microphones are well matched in both phase (with a standard deviation of 2 degrees) and magnitude. Deviations in magnitude show a standard deviation of 1.45 mV/Pa and deviations in phase show a standard deviation of 2.2 degrees. Noise measurements are shown in *Figure* 13. These results show peak noise values slightly lower than simulated results, but follow the shape of the simulated results very well. *Table* 1 summarizes the performance of the microphone array.

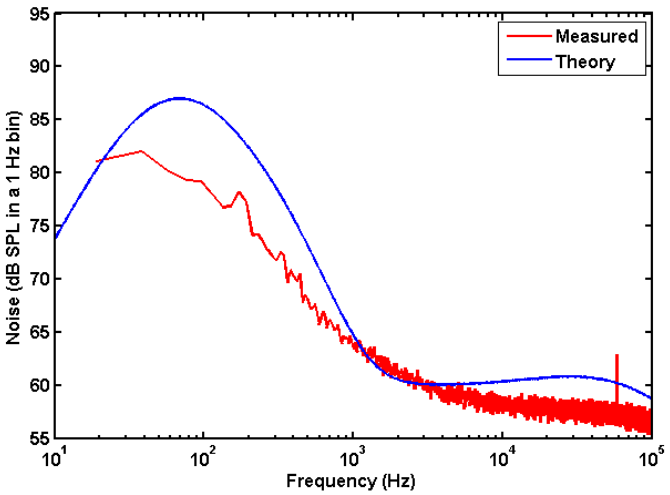

Figure 13. Measured and predicted noise density for a single microphone. Noise density is report as dB SPL with a 1 Hz bin size.

Table 1. Performance of pressure sensor array.

Performance Parameter	Device Characteristics
Sensor Chip Size	1.01 cm x 1.01 cm
Number of Elements	64
Individual Sensor Diameter	0.6 mm
Sensor Center–to–Center Spacing (Pitch)	1.2625 mm
Sensor Bandwidth	410 kHz
Sensitivity of Individual Element	0.6 mV/Pa @ $1kHz$
Sensitivity of Entire Array	38.4 mV/Pa @ $1kHz$
Center Displacement of Element	0.12 nm/V^2 @ $100kHz$
Low Frequency Rolloff	below 100 Hz
Capacitance of Each Element (including stray)	120 pF

The off chip electronics are an important part of the system design. Significant effort has been expended to reduce noise sources and cross talk between channels. As stated above, the model for the receive electronics is a series combination of two single pole passive high pass filters with break frequencies of 60 Hz and 80 Hz, a charge amplifier with a gain of 100 mV/pC, and a voltage gain stage of 100 with a single pole low pass filter at 40 kHz. The electronics circuit should gain the signal by 40 dB at the bandpass output. Isolation between channels poses the largest problem with the electronics. *Figure* 14 shows two transfer functions of the current electronics (with manual switches to turn microphones on and off) and an improved breadboarded digital switch network. The new switch network allows for each microphone to be turned off to ground which increases our off isolation by a factor of 100, but also allows for the option of beamforming through the use of inverting the signal by 180 degrees. The increase in isolation from element to element in the array will greatly improve the performance of the array.

V. Conclusion

A surface micromachined, front-vented, 64 channel (8×8), capacitively sensed pressure sensor array for aeroacoustic analysis of the turbulent boundary layer has been designed and characterized. Modeling shows an understanding of the dynamics of the sensor and anticipated results of future designs can benefit as a result of this working knowledge. The dynamics of this microphone incorporate a lumped element model

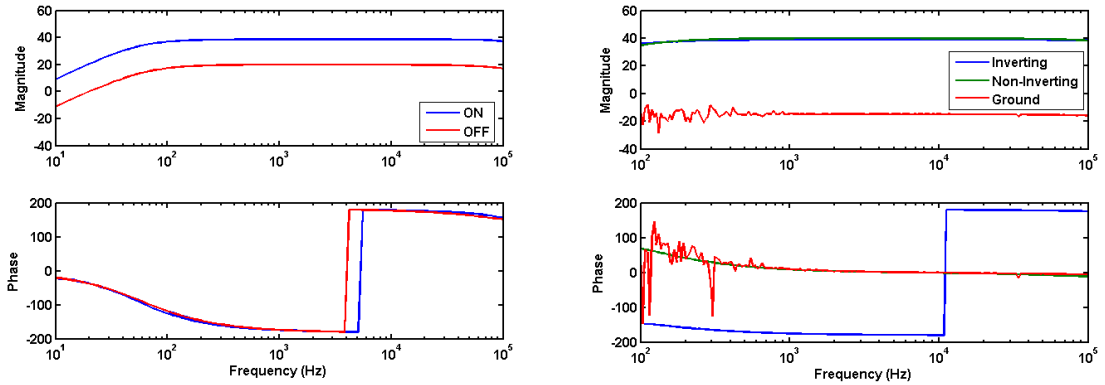

(a) (b)

Figure 14. (a) Single digital switch electronics transfer function with ON and OFF isolation. (b) Digital switch network with inverting, non-inverting, and ground connections to allow for beamforming and greater OFF isolation.

that accurately predicts the response of the microphone array using various MATLAB® scripts. Theory predicts single element sensitivity of 0.65 mV/Pa and displacement of 0.035 nm at the gain stage output in the 100-40,000 Hz band and a strong first resonance at 285 kHz.

Layout of the MEMS sensor array shows promise due to size and spatial patterning. This is the first known fine pitched MEMS pressure sensor array on a single chip with characteristic length and size scales needed for turbulent boundary layer measurements. The array is fabricated with a center–to–center pitch of 1.2625 mm allowing for low wavenumbers to be resolved by spacing multiple chips end-to-end. The fine pitch will allow for high resolution data on the frequency-wavenumber spectra of the TBL experienced by an aircraft in flight.

The pressure sensor array was fabricated using the MEMSCAP PolyMUMPs® process, along with post-processing of a polymer layer using Parylene-C. A successful 64 element, capacitively sensing pressure sensor has demonstrated acoustic sensitivity due to the fabrication techniques derived from this process. Although problems originated from fabrication flaws, knowledge of these flaws led to additional post processing which can account for these variations in fabrication processes.

Preliminary acoustic calibrations shows single element acoustic sensitivity of 0.6 mV/Pa in the 200Hz-20kHz bandwidth. A laser Doppler velocimetry (LDV) system has been used to map the spatial motion of the elements in response to electrostatic excitation. A strong resonance appears at 410 kHz from electrostatic excitation, which is in good agreement with mathematical models. Static stiffness measured electrostatically using an interferometer is 0.1 nm/V^2, similar to the expected stiffness.

Phase matching across elements in the array appears to be good (within 2 degrees). Magnitude variations are present and are under investigation. Element yield in the array is also a concern; currently we experience approximately 85% yield, which means that on the order of 5-10 microphones per 64 element chip are bad. The main yield loss appears to be at the wirebonding step. Alternative packaging methods with surface metal replacing wirebonding are under development to improve yield and reduce array surface topology. In addition, improvements to the electronics are underway to reduce noise sources and improve channel isolation. Wind tunnel testing of the array is planned in the near future.

References

[1]Tennekes, H. and Lumley, J. L., *A First Course in Turbulence*, The MIT Press, 1972.

[2]Wilby, J. F. and Gloyna, F. L., "Vibration measurements of an airplane fuselage structure II. Jet noise excitation," *Journal of Sound and Vibration*, Vol. 23, No. 4, Aug. 1972, pp. 467–486.

[3]Graham, W. R., "A Comparison of Models for the Wavenumber-Frequency Spectrum of Turbulent Boundary Layer Pressures," *Journal of Sound and Vibration*, Vol. 206, No. 4, Oct. 1997, pp. 541–565.

[4]Abraham, B. M. and Keith, W. L., "Direct Measurements of Turbulent Boundary Layer Wall Pressure Wavenumber-Frequency Spectra," *Journal of Fluids Engineering*, Vol. 120, March 1998, pp. 29–39.

[5]Corcos, G. M., "Resolution of Pressure in Turbulence," *The Journal of the Acoustical Society of America*, Vol. 35, No. 2, February 1962, pp. 192–199.

[6]Sessler, G. M., "Acoustic sensors," *Sensors and Actuators A: Physical*, Vol. 26, No. 1-3, March 1991, pp. 323–330.

[7]Scheeper, P. R., van der Donk, A. G. H., Olthuis, W., and Bergveld, P., "A review of silicon microphones," *Sensors and Actuators A: Physical*, Vol. 44, No. 1, July 1994, pp. 1–11.

[8]Löfdahl, L. and Gad-el Hak, M., "MEMS applications in turbulence and flow control," *Progress in Aerospace Sciences*, Vol. 35, 1999, pp. 101–203.

[9]Martin, D. T., Liu, J., Kadirvel, K., Fox, R. M., Sheplak, M., and Nishida, T., "A micromachined dual-backplate capacitive microphone for aeroacoustic measurements," *Journal of Microelectromechanical Systems*, Vol. 16, No. 6, 2007, pp. 1289–1302.

[10]Johnstone, R. W. and Parameswaran, M., "MUMPs Design Handbook: Unofficial Supplement," [Internet], Available at: http://www.sfu.ca/immr/, 2002.

[11]Chen, J., Liu, L., Li, Z., Tan, Z., Xu, Y., and Ma, J., "Single-Chip Condenser Miniature Microphone With High Sensitive Circular Corrugated Diaphragm," *Proceedings of the IEEE Micro Electro Mechanical Systems (MEMS)*, 2002, pp. 284–287.

[12]Beranek, L. L., *Acoustics*, Acoustical Society of America, 1996.

[13]Kinsler, L. E., Frey, A. R., Coppens, A. B., and Sanders, J. V., *Fundamentals of Acoustics: Fourth Edition*, John Wiley & Sons, 2000.

[14]Homentcovschi, D. and Miles, R., "Viscous damping of perforated planar micromechanical structures," *Sensors and Actuators A: Physical*, Vol. 119, No. 2, April 2005, pp. 544–552.